Polarization switching and high piezoelectric response in Sn-modified $BaTiO_3$

Ajay Kumar Kalyani,[1] Hari Krishnan,[2] Arijit Sen,[3] Anatoliy Senyshyn,[4] and Rajeev Ranjan[1,*]

[1]*Department of Materials Engineering, Indian Institute of Science, Bangalore, Karnataka, India*

[2]*Birla Institute of Technology and Science, Hyderabad, Andhra Pradesh, India*

[3]*Jadavpur University, Kolkata, West Bengal, India*

[4]*Forschungsneutronenquelle Heinz Maier-Leibnitz (FRM II), Technische Universität München, Lichtenbergestrasse 1, D-85747 Garching b. München, Germany*

(Received 25 April 2014; revised manuscript received 12 December 2014; published 5 January 2015)

$BaTiO_3$ is shown to exhibit anomalous piezoelectric response, comparable to that of lead-zirconate titanate, by dilute Sn modification (1–4 mol%). Using a newly discovered powder poling technique it is shown that the mechanism associated with this anomalous strain response involves electric-field-induced switching of polarization vector from [001] towards [101] pseudocubic direction. This switchability is significantly enhanced by tuning the tetragonal-orthorhombic first-order criticality near to room temperature.

DOI: 10.1103/PhysRevB.91.024101 PACS number(s): 77.22.−d, 77.80.Jk, 77.84.Cg

I. INTRODUCTION

Research on lead-free piezoelectric materials has received considerable momentum in the recent past because of serious environmental concerns with regard to the toxicity of the commercial piezoelectric, lead-zirconate titanate (PZT), which contains ∼60 wt% of lead. Lead-free compounds such as $Na_{1/2}Bi_{1/2}TiO_3$ (NBT). (K,Na)NbO_3 (KNN), and $BaTiO_3$ (BT) have been extensively investigated in pure and modified form with renewed interest [1–18]. As compared to NBT and KNN, $BaTiO_3$-based lead-free piezoelectrics have started receiving attention only in the last few years after the discovery of anomalous piezoelectric response by Liu and Ren [6] in Ca and Zr codoped $BaTiO_3$. It may be noted that a large piezoelectric response has been reported in $BaTiO_3$ single crystals by the application of a strong electric field away from the spontaneous polarization direction [16–18], analogous to the lead-based relaxor ferroelectric single crystals [19–26]. The anomalous piezoelectric response in the lead-based systems has been associated with the occurrence of monoclinic phases for compositions close to the morphotropic phase boundary [27–30]. The possibility of a stabilizing monoclinic phase in $BaTiO_3$ has been suggested by Vanderbilt and Cohen by extending the Devonshire theory to eighth order in polarization [31]. The authors listed three possible monoclinic phases and labeled them as M_A, M_B, and M_C depending on the pseudocubic plane in which the plane polarization vector is contained [31] and the two high symmetry polarization directions it bridges. For example, the polarization vector in the M_A phase lies in the pseudocubic $(1\bar{1}0)$ plane and bridges the [001] and [111] polarization directions corresponding to the tetragonal and rhombohedral phases, respectively. Using molecular dynamical simulations, Paul *et al.* have reported different monoclinic pathways $BaTiO_3$ may take during switching of polarization under an electric field [32]. The existence of local monoclinic distortion of the M_C type has recently been reported in single crystals of $BaTiO_3$ by Lummen *et al.* [33] using multiple nanoscale characterization and phase field simulation techniques. Very recently, by careful analysis of very high resolution synchrotron x-ray powder-diffraction data, we demonstrated the coexistence of a subtle monoclinic (M_C) phase along with the tetragonal phase at room temperature in polycrystalline $BaTiO_3$ and also found signatures of a field induced orthorhombic phase [34]. In the framework of polarization rotation theory the low symmetry monoclinic phase provides a continuous low energy pathway for polarization rotation on application of an electric field and constitutes the intrinsic contribution with regard to the anomalous piezoelectric response [30]. These recent observations of local monoclinic distortion in $BaTiO_3$ offers a possibility that it may be possible to tailor the system for enhanced piezoelectric response by enabling polarization switching at low energy cost.

$BaTiO_3$ exhibits three structural transitions at ∼130 °C, ∼0 °C, and ∼−90 °C [35,36]. The transition at 130 °C corresponds to ferroelectric-paraelectric tetragonal ($P4mm$)−cubic ($Pm3m$) transition. The transitions at 0 °C and −90 °C correspond to tetragonal ($P4mm$)−orthorhombic ($Amm2$) and orthorhombic ($Amm2$)−rhombohedral ($R3m$) transitions, respectively. The first-order nature of the two ferroelectric-ferroelectric transitions at 0 °C and −90 °C would ensure coexistence of ferroelectric phases around the critical temperatures, and as such, chemical modifications which can raise the tetragonal-orthorhombic transition temperature or the orthorhombic-rhombohedral transition temperature from below room temperature to close to room temperature can significantly enhance its dielectric and piezoelectric response. Interesting piezoelectric properties have been reported for Zr-modified $BaTiO_3$ [13,14] and in Ca and Zr cosubstituted $BaTiO_3$. [6–8,37] It has been reported that Zr substitution in dilute concentration (2 mol%) induces coexistence of orthorhombic and tetragonal ferroelectric phases at room temperature. The nature of coexistence changes to orthorhombic+rhombohedral above 5 mol% Zr [13,14]. Liu and Ren argued that codoping $BaTiO_3$ with Zr and Ca tunes the system towards a triple point state with drastically improved piezoelectric response [6]. In this paper we show that Sn substitution at the Ti site in dilute concentration drastically increases the piezoelectric coefficient from ∼190 pC/N to ∼425 pC/N, a value comparable to that exhibited by PZT. The system also exhibits anomalously large, nearly-hysteresis-free

*rajeev@materials.iisc.ernet.in

unipolar strain. Using a novel powder poling technique the intrinsic mechanism associated with the anomalous piezoelectric strain response was found to be switching of the polarization from [001] to [101] pseudocubic direction. This increased propensity for switching is enabled by tuning the tetragonal-orthorhombic first-order criticality close to room temperature.

II. EXPERIMENT

$Ba(Sn_xTi_{1-x})O_3$ (BTS) ceramics were prepared in close composition interval of $0 \leqslant x \leqslant 0.12$ using a solid state route. High purity $BaCO_3$, TiO_2, and SnO_2 powders were milled in planetary ball mill (P5, Fritch) using acetone medium for 10–12 h. Milled powders were dried and calcined at a temperature of 1100 °C for 4 h. Sintering was done by a two-step process: first heated to 1300 °C for 4 h and then heated to 1500 °C for 6 h. The average grain size of the sintered samples was measured using a scanning electron microscope and was found to be 60–70 μm (Fig. 1). X-ray powder-diffraction data was collected using a Bruker D8 Advance diffractometer with Cu $K\alpha$ radiation in Bragg Brentano reflection geometry. A neutron powder-diffraction (NPD) experiment was carried out at the SPODI diffractometer at FRM II, Germany using a wavelength of 1.548 Å. Dielectric measurements were done on a Novocontrol (Alpha AN) impedance analyzer. Measurement of the longitudinal piezoelectric coefficient (d_{33}) was carried out using a Berlincourt-based piezometer (Piezotest PM 300). Before the measurements the samples were poled at room temperature for ∼1 h. The polarization electric-field hysteresis loop was measured with a Radiant Precision Premier II loop tracer with MTI strain measurement setup. Rietveld refinement was carried out using FULLPROF software [38].

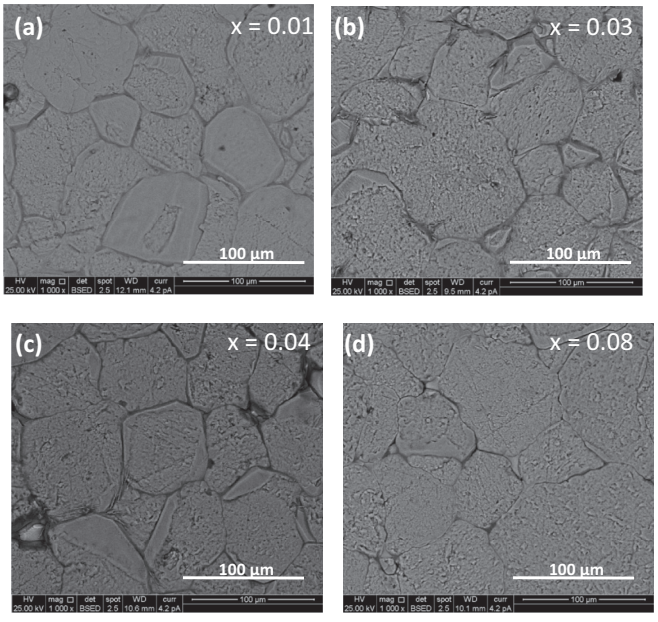

FIG. 1. Scanning electron micrographs of sintered pellets of $Ba(Ti_{1-x}Sn_x)O_3$. (a) $x = 0.01$, (b) $x = 0.03$, (c) $x = 0.04$, and (d) $x = 0.08$.

III. RESULTS

A. Piezoelectric and Ferroelectric properties

Figure 2 shows the composition variation of polarization and longitudinal piezoelectric response (d_{33}) of $Ba(Ti_{1-x}Sn_x)O_3$ (BTS) in the composition range $0 \leqslant x \leqslant 0.11$. The longitudinal piezoelectric coefficient (d_{33}) increases from 190 pC/N for pure $BaTiO_3$ to 405 pC/N at $x = 0.02$. For $x = 0.04$ and $x = 0.08$, the values are 424 and 400 pC/N, respectively. The d_{33} fall continuously after $x = 0.09$ with $d_{33} = 250$ pC/N at $x = 0.10$ and 209 pC/N at $x = 0.11$. This trend is similar to what had been reported by Yao *et al.* [39]. The remnant polarization also shows a similar trend as a function of composition [Fig. 2(b)]. Figures 2(c) and 2(d) show the variation of unipolar and bipolar strain of BTS measured at ∼50 kV/cm. A unipolar strain of 0.17% (0.21% bipolar) at $x = 0.01$ and 0.18% (0.20% for bipolar) at $x = 0.03$, which is nearly double the value obtained for pure $BaTiO_3$ (strain ∼0.1%), was achieved at a field strength of ∼50 kV/cm. The high-field strain decreases sharply for $x > 0.03$. The characteristic strain electric-field and polarization electric-field loops are shown in Figs. 2(e)–2(j). It is interesting to note that the unipolar strain curves are nearly hysteresis-free—a feature desired for high precision actuation applications. Pb-based relaxor ferroelectric PMN-PT and PZN-PT are among the known materials which exhibit hysteresis-free strain. In single crystal form the maximum strain is ∼1.7%, while in the bulk ceramic form the achievable strain is ∼0.1%. [19]. Hysteresis-free large strain is not very common among the lead-free ferroelectrics [40,41]. The reported giant strain of ∼0.45% reported in the tertiary system $Na_{1/2}Bi_{1/2}TiO_3$-$BaTiO_3$-$(K_{0.5}Na_{0.5})NbO_3$ is accompanied by an undesired large hysteresis [1] thereby limiting its practical utility. From this view, a hysteresis-free large strain of ∼0.18% in dilute "Sn" modified $BaTiO_3$ makes this system a strong lead-free contender for actuator applications.

B. Dielectric study and phase diagram

Figures 3(a)–3(e) show the temperature dependence of relative permittivity (ε') and loss tangent ($\tan\delta$) for compositions $x = 0.02$, 0.06, 0.10, 0.11, and 0.12 above room temperature. For $x = 0.02$ both ε' and $\tan\delta$ show only one anomaly at ∼120 °C corresponding to paraelectric-ferroelectric transition. For $x = 0.06$ another weak dielectric anomaly corresponding to tetragonal-orthorhombic transition became visible just above room temperature, i.e., at 35 °C. The tetragonal-cubic ferroelectric-paraelectric transition temperature, on the other hand, shifts down to 95 °C. For $x = 0.10$, all three transitions became visible above room temperature. The first anomaly at 31 °C corresponding to the rhombohedral-orthorhombic ($T_{R\text{-}O}$) transition is more prominently captured in the loss tangent plot of this composition. The other two anomalies corresponding to the orthorhombic-tetragonal transition and tetragonal-cubic transition occur at $(T_{O\text{-}T}) = 39$ °C and $T_c = 48$ °C, respectively. Accordingly, the room temperature structure of this composition should be expected as rhombohedral. The next higher composition $x = 0.11$ exhibits only one peak in the relative permitivity. However, a closer look at the loss tangent peak reveals a nearly flat

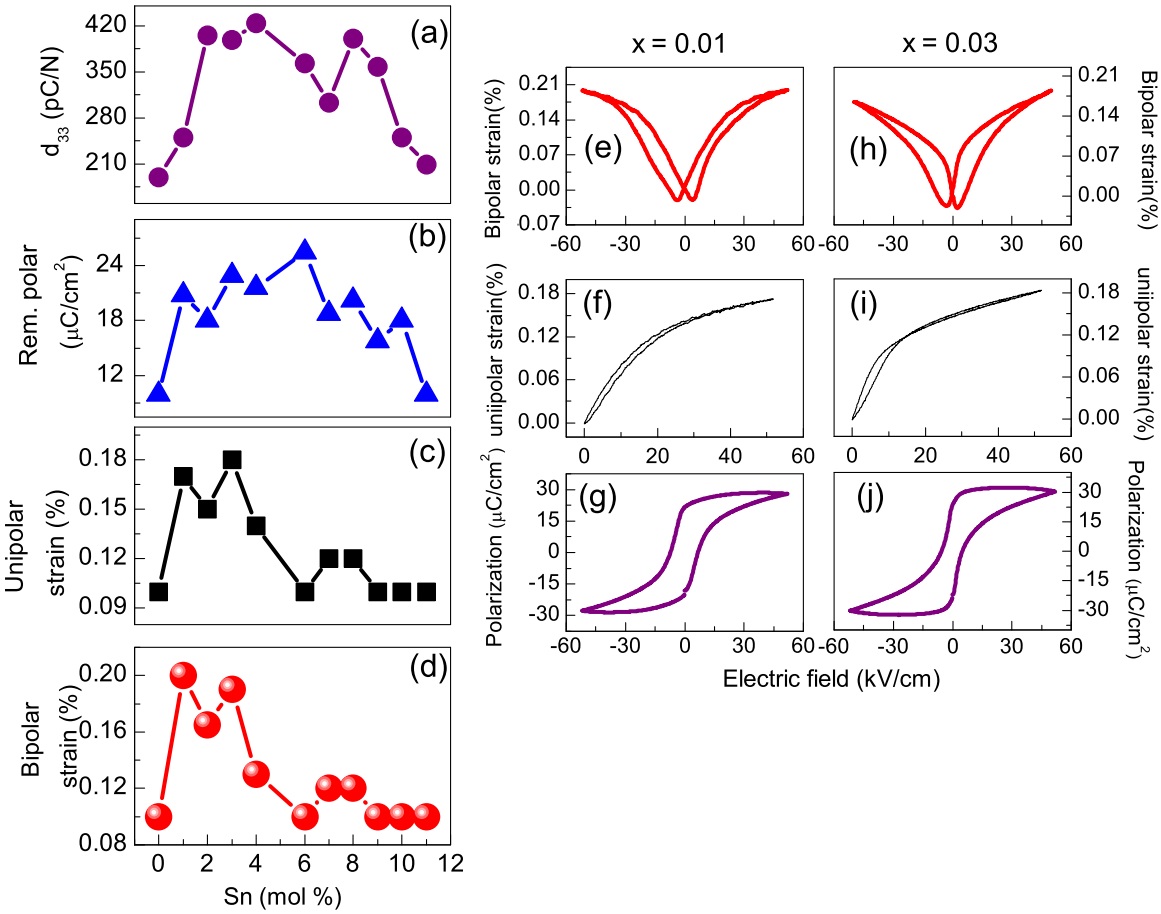

FIG. 2. (Color online) Composition dependence of (a) longitudinal direct piezoelectric coefficient d_{33}, (b) remnant polarization, (c) unipolar strain, and (d) bipolar strain. Characteristic plots of bipolar, unipolar, and remnant polarization are shown in (e)–(h) for $x = 0.01$ and 0.03 of $Ba(Ti_{1-x}Sn_x)O_3$.

top suggesting more than one transition in close proximity. The $T_{O\text{-}T}$ and $T_{O\text{-}R}$ is difficult to distinguish and may have coalesced near 32 °C. Composition $x = 0.12$ showed only one dielectric anomaly suggesting that the transitions have nearly merged for this composition. The temperature anomaly in the dielectric study was used to construct a phase diagram in the composition range $0 \leqslant x \leqslant 0.12$, Fig. 3(f). As per this phase diagram, compositions in the range $0 \leqslant x < 0.03$ should exhibit tetragonal phase at room temperature, $0.04 \leqslant x \leqslant 0.09$ should exhibit orthorhombic phase, and $0.10 \leqslant x \leqslant 0.12$ should be rhombohedral. This phase diagram also suggests that the room temperature (27 °C) becomes the critical temperature for two compositions, $x = 0.03$ corresponding to tetragonal-orthorhombic transition, and also for compositions around $x = 0.12$ where the three transitions meet. One may therefore anticipate enhanced piezoelectric/ferroelectric properties for these compositions. However, as shown in Fig. 2, the enhanced piezoelectric response occurs not only for $x = 0.03$ but in a wide composition range 0.01–0.09. For the other critical point, $x = 0.12$, the piezoelectric response is rather inferior. The dielectric based phase diagram was therefore not sufficient to explain the observed composition dependence of piezoelectric response at room temperature.

C. Structural analysis in the equilibrium state

Figures 4(a)–4(g) show the x-ray powder-diffraction profiles of three pseudocubic reflections $\{200\}_C$, $\{220\}_C$, and $\{222\}_C$ of BTS compositions in the range $0 \leqslant x \leqslant 0.11$. For the sake of direct visual comparison, Bragg profiles of unmodified $BaTiO_3$ are also given [Fig. 4(a)]. In contrast to the dielectric study, which suggests a tetragonal phase at room temperature for $x = 0.02$, the x-ray diffraction (XRD) pattern of this composition reveals an additional orthorhombic peak (marked with O). The profiles of $x = 0.04$ appear drastically different from $x = 0.02$ due to significant overlap between the tetragonal and orthorhombic peaks. The shape of the profiles continues to change gradually until $x = 0.10$ above which the changes are not visibly detectable. The singlet nature of $\{200\}_C$ and a weak doublet nature of $\{222\}_C$ in the patterns of $x = 0.10$ and $x = 0.11$ suggest the structure to be rhombohedral for these compositions. This is also consistent with the dielectric studies which suggest the rhombohedral-orthorhombic transition to occur above room temperature for these compositions (Fig. 3). The starting structural models for Rietveld fitting were chosen based on this visual analysis of the patterns. For reliable estimation of the atomic coordinates Rietveld refinement was first carried out using the neutron powder-diffraction (NPD) data. The patterns of $x = 0.02$ and $x = 0.04$ were

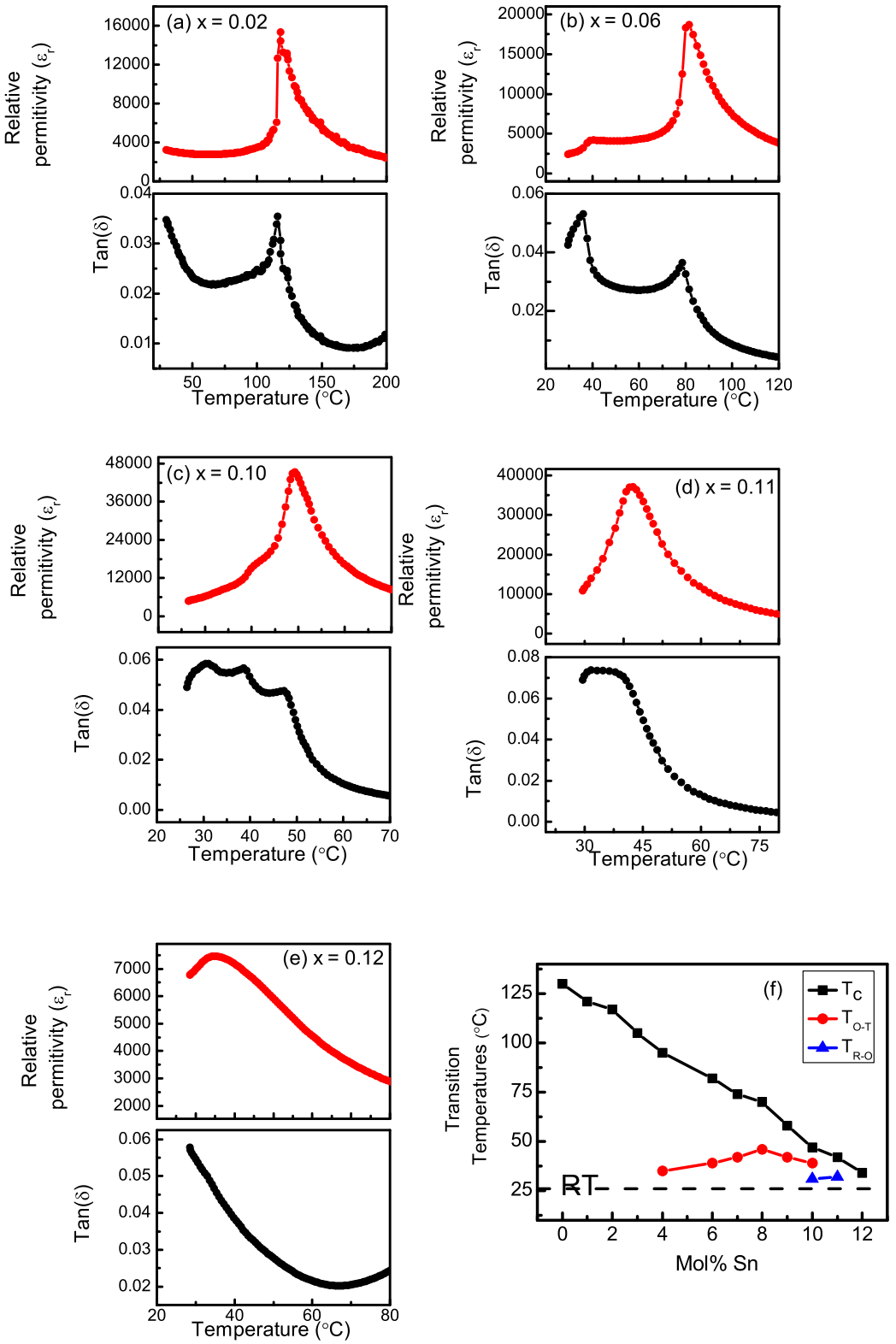

FIG. 3. (Color online) Temperature dependence of relative permittivity and loss tangent of $Ba(Ti_{1-x}Sn_x)O_3$ for (a) $x = 0.02$, (b) 0.06, (c) 0.10, (d) 0.11, and (e) 0.12. (f) shows a phase diagram constructed based on the dielectric anomalies.

fitted with tetragonal ($P4mm$) + orthorhombic ($Amm2$) phase coexistence model. Figs. 5(a–d) shows the Rietveld fitted x-ray (XRD) and NPD patterns of these compositions. The x-ray and neutron powder diffraction patterns of $x = 0.11$, on the other hand, could be fitted successfully with a single-phase rhombohedral ($R3m$) model, Figs. 5(e) and 5(f). It may be noted that due to slightly better resolution of the x-ray powder-diffraction data as compared to the neutron diffraction pattern, the onset of

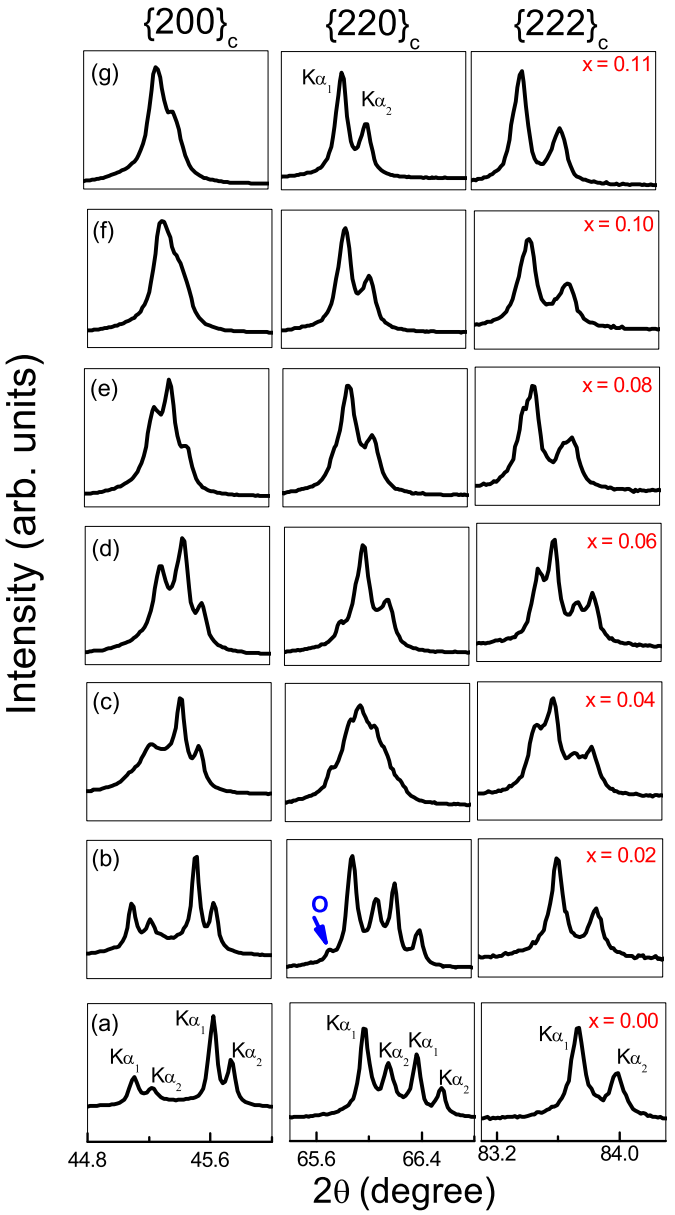

FIG. 4. (Color online) X-ray (radiation Cu $K\alpha$) powder-diffraction Bragg profiles of pseudocubic $\{200\}_c$, $\{220\}_c$, and $\{222\}_c$ reflections of $Ba(Ti_{1-x}Sn_x)O_3$. Both Cu $K\alpha_1$ and $K\alpha_2$ are present in all the diffraction profiles. The arrow points to an orthorhombic Bragg peak.

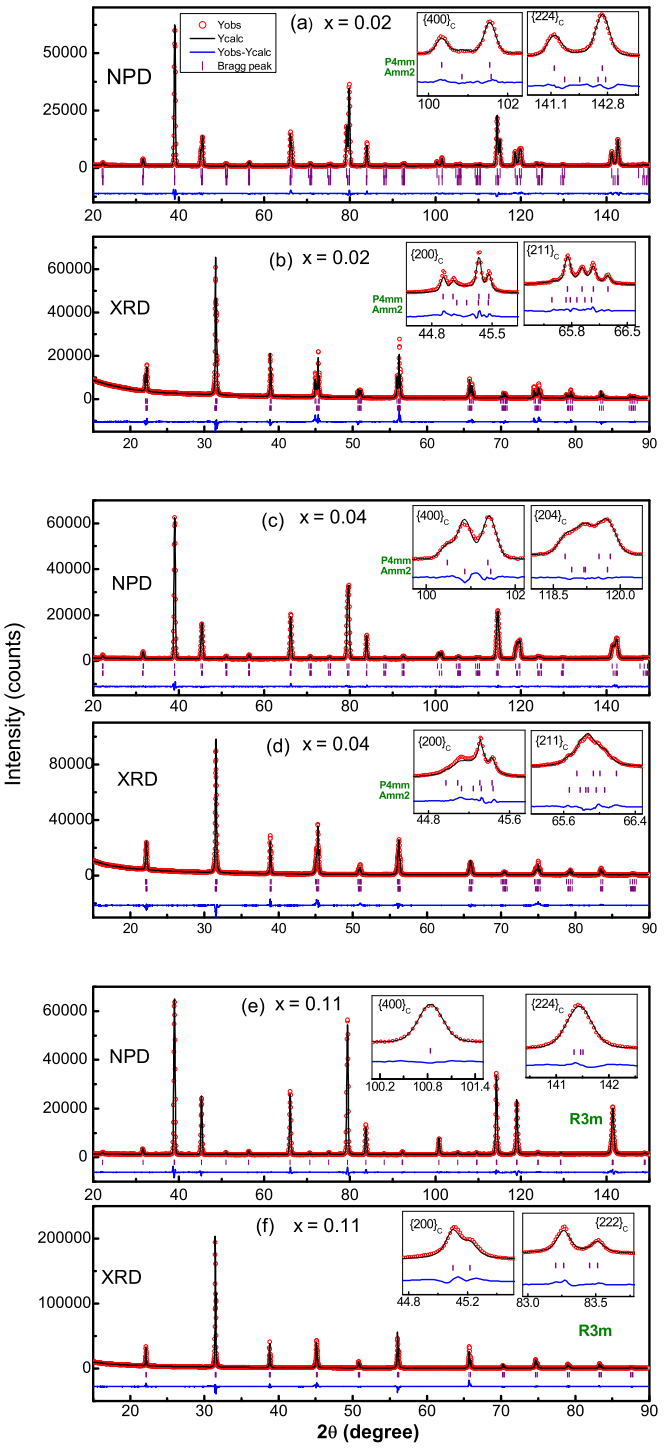

FIG. 5. (Color online) Rietveld fitted NDP and XRD patterns of $Ba(Ti_{1-x}Sn_x)O_3$ for [(a),(b)] $x = 0.02$, [(c),(d)] $x = 0.04$ using the $P4mm + Amm2$ model and [(e),(f)] for $x = 0.11$ using the $R3m$ model. The insets highlight the quality of fits by showing a magnified view of select (representative) Bragg profiles. The vertical bars indicate the calculated Bragg peak positions.

the orthorhombic peaks in $x = 0.02$ could be easily observed in the XRD pattern [see the inset of Fig. 5(b)]. For $x = 0.04$, the tetragonal and the orthorhombic peaks become clearly visible in both the x-ray and neutron powder-diffraction patterns. Table I lists the structural parameters of $x = 0.04$ using the neutron powder-diffraction data. Due to a lesser number of strong peaks in the x-ray diffraction patterns and also due to the weak scattering power of oxygen for x rays, the atomic coordinates obtained with the neutron diffraction data for $x = 0.04$ were fixed while carrying out Rietveld fitting of the x-ray diffraction data of the compositions showing $P4mm + Amm2$ phase coexistence. As evident from the insets of the figures shown in Figs. 5(a)–5(d) all the patterns fit well with the chosen $P4mm + Amm2$ two-phase model. For $x = 0.06$, while the single-phase orthorhombic structural model could fit the neutron diffraction pattern satisfactorily [Fig. 6(a)], it was not found to be satisfactory for the XRD pattern as can be seen from the inset of Fig. 6(b). The best fit of the XRD pattern of

TABLE I. Refined structural parameters and agreement factors for $Ba(Ti_{0.96}Sn_{0.04})O_3$ obtained after Rietveld refinement of neutron powder-diffraction pattern using tetragonal ($P4mm$) + orthorhombic ($Amm2$) phase coexistence model.

	Space group : $P4mm$				Space group : $Amm2$			
Atoms	x	y	z	B (Å^2)	x	y	z	B (Å^2)
Ba	0.000	0.000	0.000	0.5 (1)	0.000	0.000	0.000	0.07(9)
Ti/Sn	0.500	0.5000	0.471(2)	0.2(2)	0.500	0.000	0.495(2)	1.3(1)
O1	0.500	0.5000	0.024(1)	0.1(1)	0.000	0.000	0.498(2)	0.6(1)
O2	0.500	0.000	0.510(2)	0.5(1)	0.500	0.2577(8)	0.2371(5)	0.83(6)
$a = 4.00183(8)$ Å, $c = 4.02807(12)$ Å					$a = 3.99980(8)$ Å			
$v = 64.508(3)$ Å^3, %Phase = 39(2)					$c = 5.6754(1)$, $v = 129.096(5)$ Å^3, %Phase = 61(2)			
$R_p = 8.90$; $R_{wp} = 5.94$; $R_{exp} = 4.16$; $\chi^2 = 2.04$								

$x = 0.06$ was rather obtained with the $P4mm + Amm2$ model [inset of see Fig. 6(c)]. Due to a slightly better resolution of the XRD as compared to the NPD pattern the results of XRD analysis for the higher compositions were found to be more reliable. Figure 7 shows only the Rietveld fitted XRD patterns for $x = 0.08$. Since the composition $x = 0.08$ lies at the crossover from $P4mm + Amm2$ ($x = 0.06$) to $R3m$ ($x = 0.10$), we attempted three different structural models to fit the XRD pattern of this composition: (i) single-phase orthorhombic phase, (ii) tetragonal ($P4mm$) + orthorhombic ($Amm2$), and (iii) orthorhombic ($Amm2$) + rhombohedral ($R3m$) phase coexistence. The results are shown in Figs. 7(a)–7(c). Among all these fitted models, the tetragonal ($P4mm$) + orthorhombic ($Amm2$) phase coexistence model gave the best fit. Rietveld analysis therefore confirmed the coexistence of orthorhombic and tetragonal phases in a wide composition

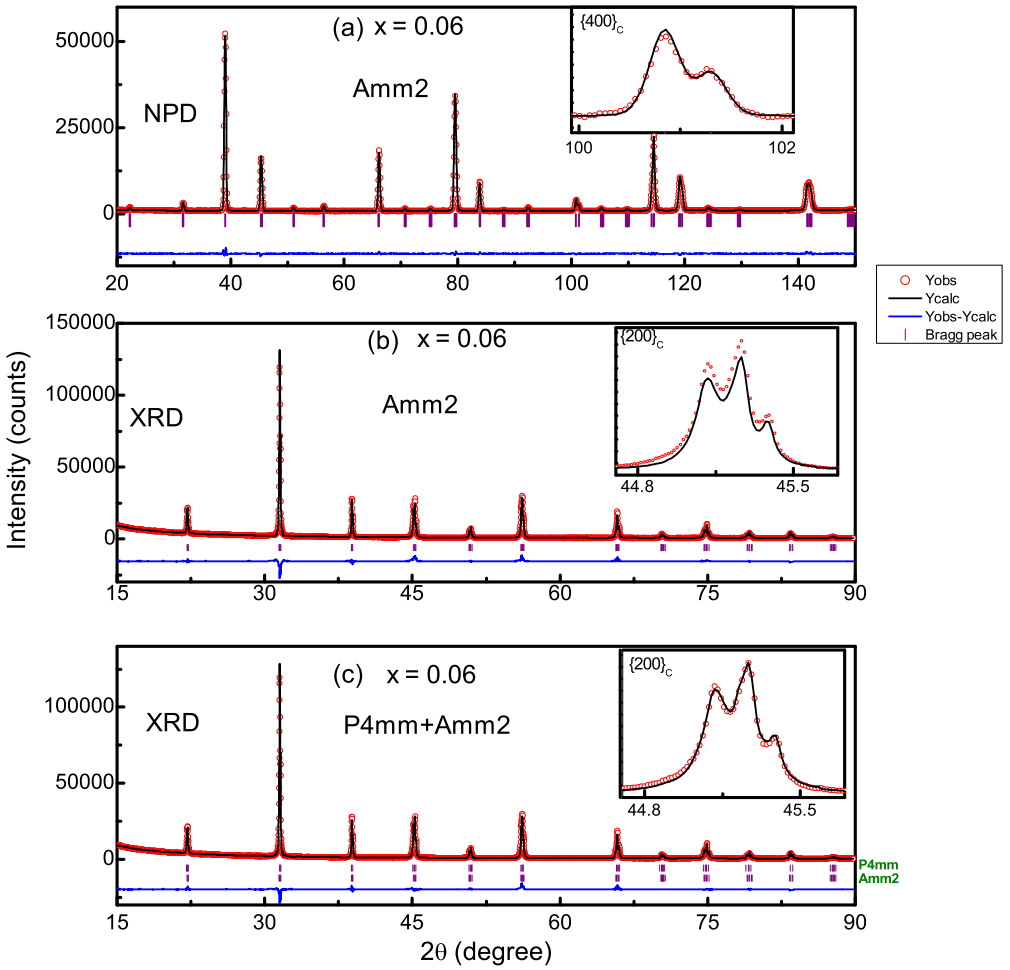

FIG. 6. (Color online) Rietveld fitted pattern for composition $x = 0.06$. (a) NPD pattern fitted with the single-phase $Amm2$ model, (b) x-ray powder-diffraction pattern fitted with the single-phase $Amm2$ model, and (c) x-ray powder-diffraction pattern fitted with the two-phase model $P4mm + Amm2$. The insets show a magnified plot of a Rietveld fitted representative pseudocubic Bragg peak.

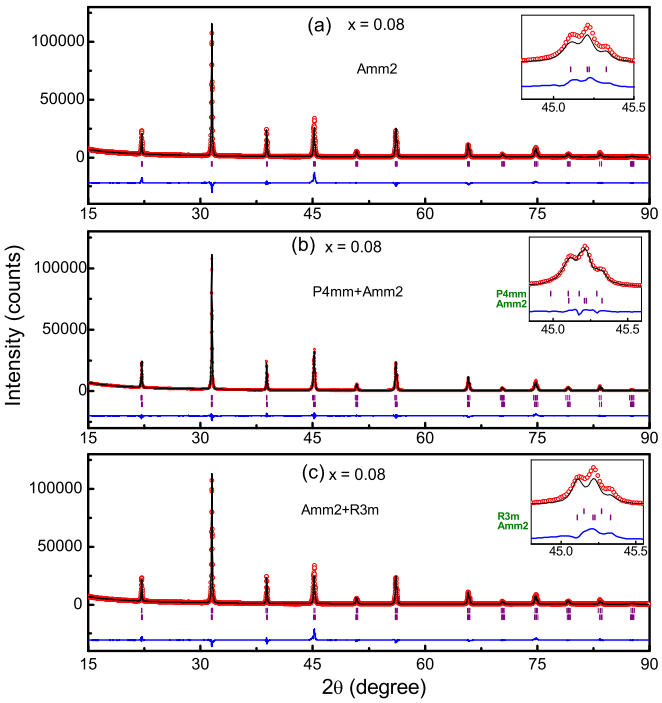

FIG. 7. (Color online) Rietveld fitted XRD patterns of $Ba(Ti_{0.92}Sn_{0.08})O_3$ with (a) $Amm2$, (b) $P4mm + Amm2$, and (c) $Amm2 + R3m$ structural models. The insets highlight the quality of fits by various models by showing a magnified view of the pseudocubic $\{200\}_c$ Bragg profile. The vertical bars indicate the calculated Bragg peak positions.

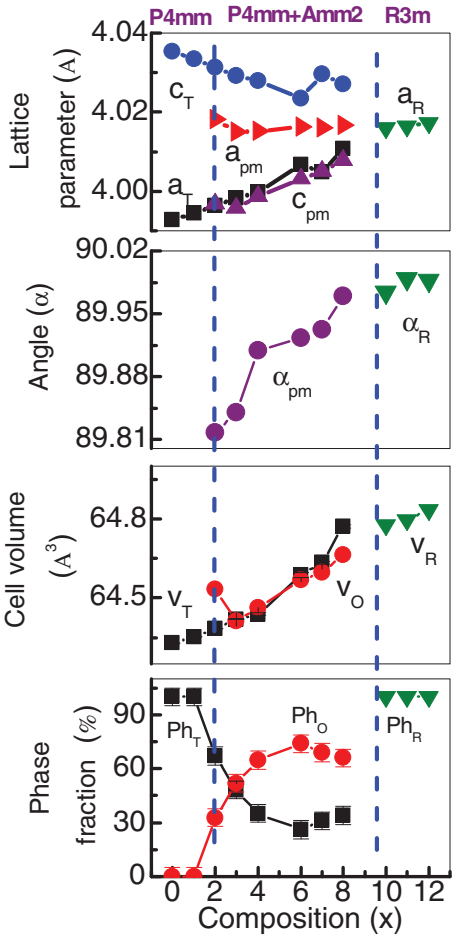

FIG. 8. (Color online) Composition dependence of lattice parameters, cell volume, and phase fractions of $Ba(Ti_{1-x}Sn_x)O_3$. For the orthorhombic structure the pseudomonoclinic lattice parameters have been plotted (see text). The subscripts T, O, R, C, and pm correspond to tetragonal, orthorhombic, rhombohedral, cubic, and pseudomonoclinic cells, respectively.

range $0.02 \leqslant x \leqslant 0.08$. Refined structural parameters of the various compositions are plotted in Fig. 8. For sake of direct comparison the orthorhombic cell parameters (a_O,b_O,c_O) were converted to the pseudomonoclinic lattice parameters $(a'_m,b'_m,c'_m,\beta'_m)$ following the relations $a_O = a'_m$, $b_O = 2c_m \sin(\alpha'_m/2)$, and $c_O = 2c_m \cos(\alpha'_m/2)$. The tetragonal lattice parameter "c" increases with composition until $x = 0.08$ while "a" decreases until $x = 0.06$ and thereafter remains nearly composition independent. The pseudomonoclinic lattice parameters "a_m," "b_m," and "α'_m" and the unit cell volume increase linearly with composition in the range $0.02 \leqslant x \leqslant 0.08$. This is anticipated since the ionic radius of "Sn" is bigger than "Ti."

D. In situ electric-field diffraction study

Figure 9 shows the evolution of the pseudocubic $\{200\}_C$ and $\{211\}_C$ Bragg profiles with increasing electric field for $x = 0.03$. These patterns were recorded on a dense ceramic pellet in reflection geometry and hence only those planes which are parallel to the pellet surface (or normal to the applied electric field) would contribute to the diffracted beam. Before application of the electric field the pseudocubic $\{200\}_C$ profile shows two tetragonal peaks, namely, $(002)_T$ and $(200)_T$ at the extreme ends, along with a peak in the middle (marked as O), corresponding to the orthorhombic phase. On the application of electric field a drastic change in the profile shape can be noticed. For example, at the field strength of 2 kV/cm the middle O peak has become stronger. At 4 kV/cm and above one can see that the intensity of the $(002)_T$ tetragonal peak increases as compared to that of the $(200)_T$ peak. This alteration is due to field induced preferred orientation caused by motion of the ferroelectric-ferroelastic domain walls in the tetragonal phase regions. Concomitantly, we can notice that the intensity of the O peak in between the $(002)_T$ and $(200)_T$ tetragonal peaks also increases. Now, as with the tetragonal phase, the electric field can also cause motion of the domain walls in the orthorhombic phase and thereby induce preferred orientation in this phase as well. One may therefore postulate that the intensity of some of the orthorhombic Bragg peaks at other positions (the position of which might be superposed with the tetragonal peaks and hence not distinctively visible) may decrease and that at the position marked as O in Fig. 9 has increased as a result of the field induced preferred orientation in the orthorhombic phase region. Further, the noticeable increase in the intensity in the middle O peak can also occur due to an increase in the orthorhombic phase fraction by the applied field. A similar type of dilemma was highlighted in another *in situ* work by Jones *et al.* on a composition close to the morphotropic phase bundary

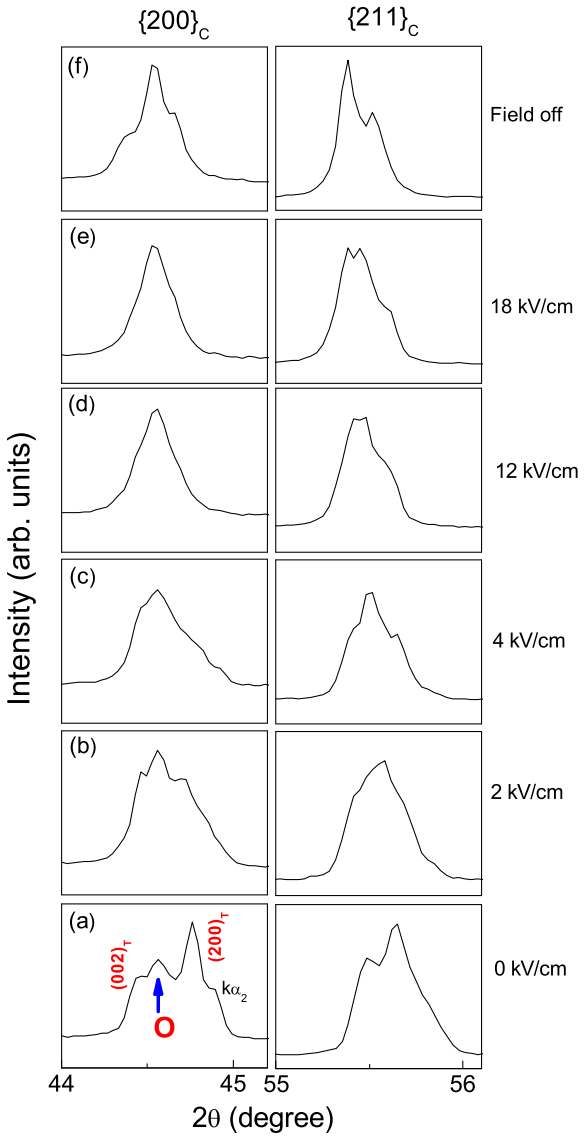

FIG. 9. (Color online) X-ray powder-diffraction Bragg profiles of the pseudocubic $\{200\}_c$ and $\{211\}_c$ obtained from a pellet subjected to *in situ* electric field. The tetragonal peaks $(002)_T$ and $(200)_T$, and the orthorhombic peak O are marked in the bottom left panel.

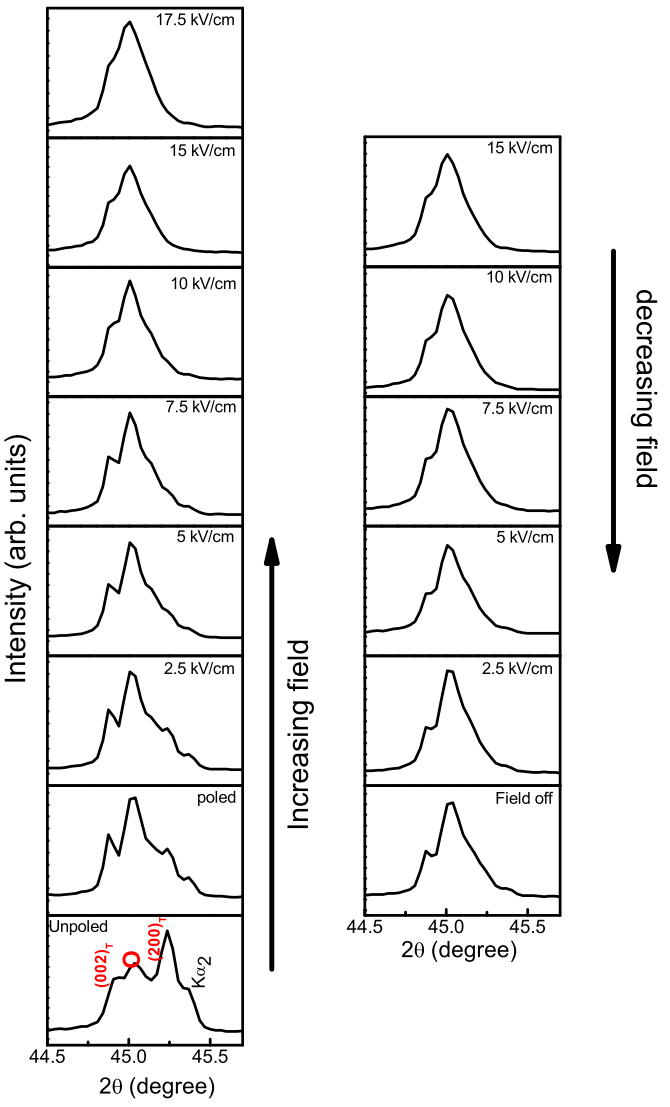

FIG. 10. (Color online) Evolution of the pseudocubic $\{200\}_C$ Bragg profile during unipolar field cycling of a poled pellet.

(MPB) of the ferroelectric system $PbTiO_3$-$BiScO_3$ [42,43]. The MPB composition of this system shows coexistence of tetragonal and monoclinic phases, and it was not possible to ascertain with certainty whether the altered intensity of the monoclinic peak on application of an electric field was due to preferred-orientation effect or because of the change in the relative fraction of the monoclinic phase. Since preferred orientation is unavoidable on application of an electric field on pellets, it is not easy to resolve such a dilemma conclusively. Reports of electric-field-induced structural transformation studies on ceramic specimens are therefore relatively few in the literature [14,23,44,45]. The majority of *in situ* diffraction studies pertain to microstructural studies (domain wall motion and strain) [46–48]. It is interesting to note that the changes in the shape of the profiles in Fig. 9 are less dramatic on increasing the field beyond the coercive limit (4 kV/cm). This suggests that the structural/microstructural evolution of the system is almost complete/saturated at this field. Above this field the changes are very small, if any, to be distinctly visible in the XRD pattern. It is important to note that the intensity of the O peak which increased while increasing the field, remains so even after switching off the field [Fig. 9(f)] thereby indicating a considerable degree of irreversibility associated with the first poling of the specimen. As stated above, while the irreversible changes in the diffraction pattern after application of a strong electric field is expected due to the irreversible motion of the ferroelectric domains (field induced preferred orientation), it will be shown below that the enhanced intensity of the O peaks after poling also has a contribution from increased volume fraction of the orthorhombic phase. In a subsequent experiment we carried out a diffraction study while increasing and decreasing the electric field on an already poled pellet to understand the structural and microstructural basis of the nearly-hysteresis-free unipolar strain electric-field response exhibited by $x = 0.03$. Figure 10 shows the evolution of the pseudocubic $\{200\}$ Bragg profile during field cycling of a poled pellet. In accordance with the *in situ* study the poled

pellet shows the strongest intensity for the O peak and altered intensity ratio of the $(002)_T$ and $(200)_T$ tetragonal peaks due to preferred orientation resulting from irreversible motion of the domain walls. The intensity of the $(200)_T$ appears significantly suppressed at 5 kV/cm and above. The profile shape is not noticeably affected at higher fields. The maximum field we went up to was 17.5 kV/cm. Subsequently, we recorded the profile evolution during decreasing the field. The profile shape at a given field during the decreasing field can be seen to be nearly identical to that obtained at that field while increasing the field. This near reversibility of the pattern is proof of the reversibility of the structural and microstructural changes during the unipolar field cycling. The main reason for this reversibility lies in the fact that the structural and microstructural changes are almost frozen once the system has been poled, and during the next unipolar cycle the field induces nearly reversible structural and microstructural changes.

E. A new powder poling technique

Though the *in situ* diffraction study could qualitatively explain a one-to-one correspondence between the nearly-hysteresis-free unipolar strain field response, it was not possible to ascertain the nature of field induced structural transformation, if any, because the severe preferred-orientation effect present in the diffraction data made it unworthy for Rietveld analysis. This inherent problem was resolved by adopting an innovative strategy of subjecting powder specimens to a high electric field and carrying out diffraction studies on these powders to unravel the nature of the field induced structural changes. This new technique is *ex situ* based, and the central idea is to capture the residual irreversible structural change after subjecting the powder specimen to a strong electric field. Since, as shown above, the profile shapes are irreversibly changed after removal of the field, and that if this change is also associated with irreversible structural changes, then the nature of irreversible change can be captured by undertaking an x-ray diffraction study on a powder specimen which has been subjected to a strong electric field. While the randomness of the orientation of the crystallites of the powder will ensure that the preferred-orientation effect is nullified, the information with regard to the nature of structural transformation induced by the field will be retained in the poled crystallites of the powder and can be retrieved by Rietveld fitting of the preferred orientation free diffraction data. This idea led us to develop the powder poling technique.

The powder for the powder poling was obtained by manual crushing of sintered pellets. The ground powder was sufficiently annealed to get rid of stress induced changes incurred in the system during the grinding operation. The annealed powder was then gently mixed with 1–2 wt% of acryl polymer powder. This mixture was compacted in the form of a green pellet. The green compact of ceramic+polymer was gently wetted drop by drop with acrylic acid. The wet compact was allowed to dry (curing) at room temperature for ~24 h. The dried compact became a mechanically hard solid. To ensure that the powder particles inside the composite were free from the stress induced changes, if any, during the compaction of the green composite, the dried compact was heated to 200 °C for 1 h. In a separate experiment we recovered the powder after this treatment (i.e., heating the compact to 200 °C) by dissolving the compact in acetone and found the diffraction pattern of the powder thus recovered to be exactly the same as the annealed powder we started with. Henceforth, any change in the structure after subjecting the heat treated composite to a high electric field can be unambiguously attributed to the pure electric field effect. Since the applied voltage would drop relatively more in the polymer region of the polymer+ferroelectric composite, the field experienced by the actual ferroelectric component is likely to be much lower. Keeping this in view, the composite was subjected to an electric field much in excess of the coercive field of the ferroelectric ceramic. In the present case, the composite was subjected to a field of ~40 kV/cm, which is about ten times the coercive field of the ferroelectric component (~4 KV/cm) to ensure that the ferroelectric particles experience a sufficient field to exhibit phase transformation. After poling the heated compact at room temperature, the compact was dissolved in acetone to retrieve the ceramic powder. The powder thus obtained is termed as "poled powder." The randomness of the crystallites in the poled powder specimen ensured a preferred-orientation free diffraction pattern which was used to determine with accuracy the nature of the irreversible structural changes brought about by the poling field, as detailed in the next section.

F. Evidence of field induced tetragonal to orthorhombic transformation

Figures 11(a)–11(d) show a magnified view of two representative Rietveld fitted x-ray pseudocubic Bragg profiles of the annealed and powder poled specimens of $x = 0.03$, 0.04, 0.06, and 0.10. The fitting of the entire diffraction pattern for the various compositions was carried out as per the structural models discussed in Sec. III C. The annealed specimen represents the equilibrium state and serves as the reference with respect to which field induced structural changes can be determined. A visual comparison of the profiles of the annealed and the poled specimens clearly reveals a distinct increase in the intensity of the O peak for the composition $x = 0.03$. On the other hand, the change in the relative intensity of the O peak is less distinct for the higher compositions, $x = 0.04$, 0.06, and 0.10, Figs. 11(b)–11(d). The change in the fraction of the orthorhombic and tetragonal phases after poling the powders of $x = 0.03$, 0.04 and 0.06 were determined by Rietveld analysis of the patterns using the $P4mm + Amm2$ phase coexistence model. Table II lists the percentage changes in the lattice parameters and phase fractions of $x = 0.03$, 0.04, 0.06, and 0.10 after poling. The maximum change (increase ~0.1%) was found in the c parameter of the tetragonal phase for all the three compositions, $x = 0.03$, 0.04, and 0.06, exhibiting phase coexistence. The most remarkable change which is distinctive of $x = 0.03$ turns out to be an increase in the orthorhombic phase fraction by 27%. For the other compositions this increase is less than 5%. Thus, there seems to be a correspondence between the propensity of the system for field induced tetragonal to orthorhombic phase transformation and the high field strain.

TABLE II. Lattice parameters, cell volume, and volume fractions of the phases in the annealed and poled Sn-modified $BaTiO_3$ powder.

	*Amm*2			*P*4*mm*		
Parameter (L)	Annealed (A)	Poled (P)	$(\Delta L_P/L_A) * 100$	Annealed (A)	Poled (P)	$(\Delta L_P/L_A) * 100$
$x = 0.03$						
a (A)	3.99856(3)	3.99649(7)	0.052	3.99825(7)	3.9998(3)	0.039
b (A)	5.6784(5)	5.6782(1)	0.003			
c (A)	5.6833(9)	5.6829(2)	0.007	4.02968(9)	4.0347(5)	0.12
Volume (A^3)	129.04(3)	128.962(5)	0.06	64.419(2)	64.55(1)	0.20
Phase %	52(1)	78(1)		48(1)	22(1)	
$x = 0.04$						
a (A)	3.99866(3)	3.99854(4)	−0.002	3.99974(1)	4.00127(8)	0.034
b (A)	5.6737(1)	5.6706(3)	0.055			
c (A)	5.6827(9)	5.6822(4)	−0.008	4.0279(9)	4.03281(3)	0.12
Volume (A^3)	128.925(3)	128.958(5)	0.03	64.438(5)	64.582(4)	0.22
Phase %	65(1)	64(1)		35(1)	36(1)	
$x = 0.06$						
a (A)	4.0034(3)	4.0043(2)	0.021	4.0078(2)	4.0064(2)	−0.006
b (A)	5.6784(2)	5.6804(2)	−0.035			
c (A)	5.6829(3)	5.6867(2)	0.065	4.0305(8)	4.0379(3)	0.18
Volume (A^3)	129.189(3)	129.349(5)	0.16	64.438(5)	64.582(4)	0.11
Phase %	74(1)	80(1)		26(1)	20(1)	
$x = 0.10$						
a (A)	4.0170(2)	4.0148(3)	−0.055			
b (A)	89.975(5)	90.012(5)	0.041			
Volume (A^3)	64.821(3)	64.714(5)	−0.16			

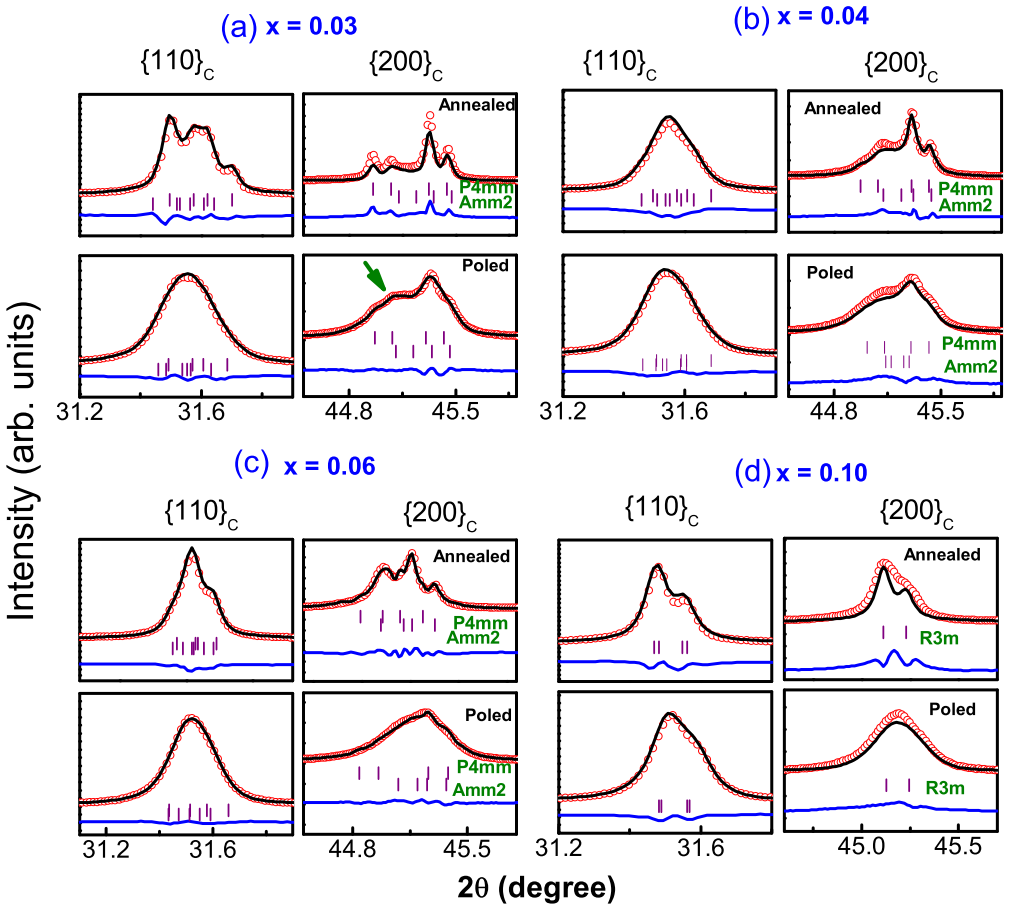

FIG. 11. (Color online) X-ray powder-diffraction Bragg profiles of pseudocubic $\{110\}_c$ and $\{200\}_c$ reflections of $Ba(Ti_{1-x}Sn_x)O_3$ in the annealed and the powder poled state for (a) $x = 0.03$, (b) $x = 0.04$, (c) $x = 0.06$, and (d) for $x = 0.10$.

IV. DISCUSSION

The coexistence of ferroelectric phases, i.e., the MPB state, for realization of enhanced piezoelectric response in piezoceramics is considered an essential requirement. The MPB is a composition induced first-order ferroelectric-ferroelectric instability. The anisotropic flattening of the energy profile near the criticality provides a low energy pathway for polarization rotation and constitutes the intrinsic mechanism for piezoelectric response [49]. The polarization rotation is facilitated by the low symmetry monoclinic phases as this structure provides the pathway for continuous rotation of the polarization vector within the mirror plane. Although the genuinity of the reported monoclinic phase in high performance lead-based piezoelectrics has been questioned by adaptive phase theory which believes that the perceived monoclinic phase is due to coherent scattering by suitably oriented nanosized domains of the high symmetry (tetragonal or rhombohedral) phase [50,51], the presence of a genuine monoclinic phase cannot be ruled out. First-principles and phenomenological calculations on single domain perovskite ferroelectrics have indeed shown that monoclinic phases are possible [29,31]. TEM studies by Sato *et al.* [52], Morozumi *et al.* [53], and Schierholz *et al.* [54] have confirmed the presence of nanosized monoclinic domains in lead-based MPB systems. Ge *et al.* [55] have reported the presence of monoclinic distortion in a multicomponent (Na,K)(Nb,Sb)-$LiTaO_3$-$x$$BaZrO_3$ lead-free system using high resolution synchrotron XRD and, in analogy with the lead-based piezoelectrics, have attributed the enhanced piezoelectric response ($d_{33} \sim 365$ pC/N) to the mechanism of polarization rotation in the monoclinic phase. Lummen *et al.* [33] and Kalyani *et al.* [34] have recently shown the existence of weak monoclinic distortion even in pure $BaTiO_3$ at room temperature. The monoclinic distortion was identified as M_C type (space group Pm). In the framework of polarization rotation theory this monoclinic phase can be considered as a structural bridge connecting the tetragonal and the orthorhombic phases. As shown in the schematic diagram in Fig. 12, the polarization can rotate in the pseudocubic $(010)_c$ mirror plane and in its extreme departure from the $[001]_c$ direction (corresponding to the tetragonal phase), it will be oriented along the $[101]_c$ (corresponding to the orthorhombic phase) [31]. The significant increase in the orthorhombic fraction after poling as evident from the powder poling experiment on $x = 0.03$ is indicative of the considerably enhanced propensity for the polarization switching from $[001]_c$ to $[101]_c$ on application of field. Paul *et al.* have argued that the switching propensity is enhanced by intermediate monoclinic regions [32]. Though the diffraction data in our case could be fitted satisfactorily with tetragonal and orthorhombic phase coexistence models, the presence of very weak monoclinic distortion cannot be ruled out completely until very high resolution diffraction experiments are carried out [34]. Davis *et al.* [24] have argued that for situations when the polarization is not exactly along either [001] or [101] but very close to them, the associated monoclinic distortion of the unit cell may not be detected in diffraction experiments. In such situations structures might as well be referred to as pseudotetragonal or pseudo-orthorhombic [24].

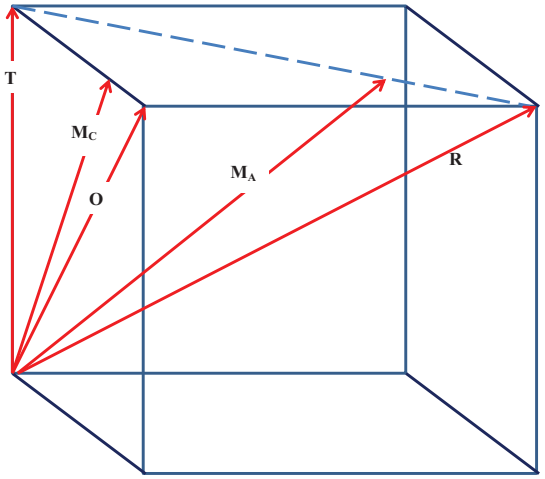

FIG. 12. (Color online) Schematic of the polarization rotation model. The polarization vectors in the tetragonal (T), orthorhombic (O), and rhombohedral (R) phases are shown. The monoclinic (M_C) phase is represented by a polarization vector in the $(010)_C$ plane. The polarization vector in the $(1\bar{1}0)_C$ plane represents the M_A monoclinic phase.

Using time resolved neutron diffraction experiments, Jones *et al.* [42,43] have argued that the significant contribution to the overall piezoelectric response at subcoercive field amplitudes also comes from motion of domain walls in both the coexisting (tetragonal and monoclinic) phases. It may be pointed out that for the MPB systems the ferroelectric phases are nearly degenerate and even small fields are likely to tilt the energy balance in favor of one of the coexisting phases resulting in a field induced transformation. Since field induced transformation would involve the creation and movement of interferroelectric boundaries, it is evident that the overall piezoelectric response would have a significant contribution, not only from the motion of domain walls but also to interferroelectric boundaries. Studies in the past have not, however, given due consideration to the role of interphase boundaries in MPB based piezoelectric systems presumably due to the difficulty associated with their accurate characterization. Our innovative powder poling experiment has clearly shown the phenomenon of field induced tetragonal to orthorhombic transformation. For composition close to the tetragonal-orthorhombic criticality this transformation is significantly irreversible—27 percent of the tetragonal fraction has irreversibly converted to orthorhombic for $x = 0.03$. Signature of a large degree of irreversible changes is also noted in the *in situ* field dependent diffraction experiment on an unpoled pellet of $x = 0.03$ (Fig. 9). The nature of the irreversible structural transformation is expected to be the same in the powder as well as in the pellet specimens. Since the alteration in the ratio of the tetragonal $(002)_T$ and $(200)_T$ peaks occur (as evident from the *in situ* experiment on the pellet, Fig. 9) along with the decrease in the fraction of the tetragonal phase (as evident from the powder poling experiment), it is evident that domain wall motion and creation/motion of interphase boundaries happens simultaneously. The movement of these

two different types of boundaries cannot be independent of each other and is expected to be highly interlinked.

It is also possible that electric field not only moves an existing interphase boundary, but creates a new interphase by nucleating another ferroelectric phase well within the region of a preexisting phase. Computational studies by Rao and Wang [12] have revealed that in domain engineered single crystals where the domain wall mobility is frozen, application of an electric field broadens the domain walls and may also nucleate a new phase in the wall region. These changes are of reversible nature and hence the associated piezoelectric response will also be reversible. Since our specimen is not single crystal but ceramic, with grains oriented in all possible directions, the domain engineering concept does not directly apply here. However, the fact that the first application of an electric field leads to a considerable irreversible microstructural and structural change in the virgin (unpoled) pellet, is akin to the situation of near freezing of the domains in the domain engineered single crystals (Fig. 9). The scope of further large structural and microstructural changes is reduced on such a poled pellet. As in the case with domain engineered single crystals, the unipolar field on such a poled pellet would bring about small reversible motion domain walls, their broadening, or even field induced transformation. The mechanisms operating in the system may vary in different electric-field regimes leading to nonlinear field dependence of strain response on going from low fields to high fields. However, the reversibility of the mechanisms in the different field regions would ensure the near reversibility in the piezoelectric strain at all fields. This seems to be the reason for the nearly hysteresis-free electric-field strain response in the unipolar measurements (Fig. 3). The fact that large high-field strain is observed only for the limited composition range $0.01 < x < 0.03$ [Figs. 2(c) and 2(d)], whereas the weak-field direct piezoelectric response remains large in a broader composition range $0.01 < x < 0.08$ [Fig. 2(a)] can be attributed to the decrease in the propensity of field induced polarization switching at higher fields for $x > 0.03$. Interestingly our previous studies on Zr-modified $BaTiO_3$ [13,14] also showed an enhanced weak-field direct piezoelectric response (as measured by a Berlincourt-based piezometer) in the same composition range $0.01 < x < 0.08$. The ferroelectric phases coexist in this composition range for the Zr-modified system as well. This correlation suggests that the mechanism associated with the weak-field direct piezoelectric coefficient is similar in both the systems.

V. CONCLUSIONS

In conclusion, we show that dilute Sn modification of $BaTiO_3$ can lead to an anomalous increase in its piezoelectric properties, comparable to lead-zirconate titanate. The system also shows large piezostrain in a narrow composition interval of 0.01–0.03. Using a newly developed technique of powder poling, this anomalous response is associated with an enhanced propensity of electric-field-induced switching of polarization from [001] to [101] pseudocubic direction. The energy cost for polarization switching seems to be drastically reduced by bringing the first-order tetragonal-orthorhombic criticality from below room temperature to close to room temperature.

ACKNOWLEDGMENTS

R.R. acknowledges financial support from SERB of the Department of Science and Technology, Government of India (Grant No. SERB/F/5046/2013-14), and from the ISRO-IISc, Space Technology Cell.

[1] S.-T. Zhang, A. B. Kounga, E. Aulbach, H. Ehrenberg, and J. Rödel, Appl. Phys. Lett. **91**, 112906 (2007).
[2] W. Jo, T. Granzow, E. Aulbach, J. Rödel, and D. Damjanovic, J. Appl. Phys. **105**, 094102 (2009).
[3] J. Rödel, W. Jo, K. T. P. Seifert, E.-M. Anton, T. Granzow, and D. Damjanovic, J. Am. Ceram. Soc. **92**, 1153 (2009).
[4] B. N. Rao and R. Ranjan, Phys. Rev. B **86**, 134103 (2012).
[5] R. Garg, B. N. Rao, A. Senyshyn, P. S. R. Krishna, and R. Ranjan, Phys. Rev. B **88**, 014103 (2013).
[6] W. Liu and X. Ren, Phys. Rev. Lett. **103**, 257602 (2009).
[7] D. Xue, Y. Zhou, H. Bao, J. Gao, C. Zhou, and X. Ren, Appl. Phys. Lett. **99**, 122901 (2011).
[8] C. Zhou, W. Liu, D. Xue, X. Ren, H. Bao, J. Gao, and L. Zhang, Appl. Phys. Lett. **100**, 222910 (2012).
[9] Y. Gao, J. Zhang, Y. Qing, Y. Tan, Z. Zhang, and X. Hao, J. Am. Ceram. Soc. **94**, 2968 (2011).
[10] W. Ge, J. Li, D. Viehland, Y. Chang, and G. L. Messing, Phys. Rev. B **83**, 224110 (2011).
[11] X. Ren, Nat. Mater. **3**, 91 (2004).
[12] W.-F. Rao and Y. U. Wang, Appl. Phys. Lett. **90**, 041915 (2007).
[13] A. K. Kalyani, A. Senyshyn, and R. Ranjan, J. Appl. Phys. **114**, 014102 (2013).
[14] A. K. Kalyani and R. Ranjan, J. Phys.: Condens. Matter **25**, 362203 (2013).
[15] R. Chu, Z. Xu, G. Li, H. Zeng, H. Yu, H. Luo, and Q. Yin, Appl. Phys. Lett. **86**, 012905 (2005).
[16] S.-E. Park, S. Wada, L. E. Cross, and T. R. Shrout, J. Appl. Phys. **86**, 2746 (1999).
[17] S. Wada, K. Yako, H. Kakemoto, T. Tsurumi, and T. Kiguchi, J. Appl. Phys. **98**, 014109 (2005).
[18] H. Cao, C. P. Devreugd, W. Ge, J. Li, D. Viehland, H. Luo, and X. Zhao, Appl. Phys. Lett. **94**, 032901 (2009).
[19] S.-E. Park and T. R. Shrout, J. Appl. Phys. **82**, 1804 (1997).
[20] S. F. Liu, S. E. Park, T. R. Shrout, and L. E. Cross, J. Appl. Phys. **85**, 2810 (1999).
[21] M. Davis, D. Damjanovic, and N. Setter, J. Appl. Phys. **97**, 064101 (2005).
[22] B. Noheda, Z. Zhong, D. E. Cox, G. Shirane, S-E. Park, and P. Rehrig, Phys. Rev. B **65**, 224101 (2002).
[23] B. Noheda, D. E. Cox, G. Shirane, S.-E. Park, L. E. Cross, and Z. Zhong, Phys. Rev. Lett. **86**, 3891 (2001).
[24] M. Davis, D. Damjanovic, and N. Setter, Phys. Rev. B **73**, 014115 (2006).
[25] F. Bai, N. Wang, J. Li, D. Viehland, P. M. Gehring, G. Xu, and G. Shirane, J. Appl. Phys. **96**, 1620 (2004).

[26] F. Bai, J. Li, and D. Viehland, J. Appl. Phys. **97**, 054103 (2005).
[27] A. K. Singh and D. Pandey, Phys. Rev. B **67**, 064102 (2003).
[28] R. Guo, L. E. Cross, S.-E. Park, B. Noheda, D. E. Cox, and G. Shirane, Phys. Rev. Lett. **84**, 5423 (2000).
[29] L. Bellaiche, A. Garcia, and D. Vanderbilt, Phys. Rev. B **64**, 060103(R) 2001
[30] H. Fu and R. E. Cohen, Nature (London) **403**, 281 (2000).
[31] D. Vanderbilt and M. H. Cohen, Phys. Rev. B **63**, 094108 (2001).
[32] J. Paul, T. Nishimatsu, Y. Kawazoe, and U. V. Waghmare, Phys. Rev. B **80**, 024107 (2009).
[33] T. T. A. Lummen, Y. Gu, J. Wang, S. Lei, F. Xue, A. Kumar, A. T. Barnes, E. Barnes, S. Denev, A. Belianinov, M. Holt, A. N. Morozovska, S. V. Kalinin, L.-Q. Chen, and V. Gopalan, Nat. Commun. **5**, 3172 (2014).
[34] A. K. Kalyani, D. Khatua, B. Loukya, R. Datta, A. N. Fitch, A. Senyshyn, and R. Ranjan, arXiv:1409.1692.
[35] B. Jaffe, W. R. Cook, and H. Jaffe, *Piezoelectric Ceramics* (Academic, New York, 1971).
[36] G. H. Kwei, A. C. Lawson, S. J. L. Billinge, and S. W. Cheong, J. Phys. Chem. **97**, 2368 (1993).
[37] D. Xue, Y. Zhou, H. Bao, C. Zhou, J. Gao, and X. Ren, J. Appl. Phys. **109**, 054110 (2011).
[38] J. Rodrigues-Carvajal, *FULLPROF: A Rietveld Refinement and Pattern Matching Analysis Program* (Laboratories Léon Brillouin (CEA-CNRS), France, 2000).
[39] Y. Yao, C. Zhou, D. Lv, D. Wang, H. Wu, Y. Yang, and X. Ren, Europhys. Lett. **98**, 27008 (2012).
[40] C. Ang, Z. Yu, Z. Jing, R. Guo, A. S. Bhalla, and L. E. Cross, Appl. Phys. Lett. **80**, 3424 (2002).
[41] Z. Yu, C. Ang, R. Guo, and A. S. Bhalla, J. Appl. Phys. **92**, 1489 (2002).
[42] J. L. Jones, E. Aksel, G. Tutuncu, T.-M. Usher, J. Chen, X. Xing, and A. J. Studer, Phys. Rev. B **86**, 024104 (2012).
[43] G. Tutuncu, D. Damjanovic, J. Chen, and J. L. Jones, Phys. Rev. Lett. **108**, 177601 (2012).
[44] M. Hinterstein, J. Rouquette, J. Haines, P. Papet, M. Knapp, J. Glaum, and H. Fuess, Phys. Rev. Lett. **107**, 077602 (2011).
[45] K. A. Schönau, M. Knapp, H. Kungl, M. J. Hoffmann, and H. Fuess, Phys. Rev. B **76**, 144112 (2007).
[46] A. Pramanick, D. Damjanovic, J. E. Daniels, J. C. Nino, and J. L. Jones, J. Am. Ceram. Soc. **94**, 293 (2011).
[47] M. J. Hoffmann, M. Hammer, A. Endriss, and D. C. Lupascu, Acta Mater. **49**, 1301 (2001).
[48] J. L. Jones, A. Pramanick, J. C. Nino, S. M. Motahari, E. Ustundag, M. R. R. Daymond, and E. C. Oliver, Appl. Phys. Lett. **90**, 172909 (2007).
[49] D. Damjanovic, J. Am. Ceram. Soc. **88**, 2663 (2005).
[50] Y. M. Jin, Y. U. Wang, A. G. Khachaturyan, J. F. Li, and D. Viehland, Phys. Rev. Lett. **91**, 197601 (2003).
[51] Y. M. Jin, Y. U. Wang, A. G. Khachaturyan, J. F. Li, and D. Viehland, J. Appl. Phys. **94**, 3629 (2003).
[52] Y. Sato, T. Hirayama, and Y. Ikuhara, Phys. Rev. Lett. **107**, 187601 (2011).
[53] K. Morozumi, J. Kato, Y. Kawakubo, and S. Denda, Jpn. J. Appl. Phys. **45**, 6365 (2006).
[54] R. Schierholz, H. Fuess, K. Tsuda, Y. Ogata, M. Terauchi, and R. Theismann, Phys. Rev. B **78**, 024118 (2008).
[55] W. Ge, Y. Ren, J. Zhang, C. P. Devreugd, J. Li, and D. Viehland, J. Appl. Phys. **111**, 103503 (2012).